



# Response of *Pinus sylvestris* var. *mongolica* to water change and the reconstruction of drought history for the past 260 years in northeast China

1 Liangjun Zhu<sup>1,2</sup>, Qichao Yao<sup>1</sup>, David J. Cooper<sup>2</sup>, Shijie Han<sup>3</sup>, Xiaochun Wang<sup>1\*</sup>

2 <sup>1</sup>College of forestry, Northeast Forestry University, Harbin 150040, China

3 <sup>2</sup>Department of Forest and Rangeland Stewardship, Colorado State University, Fort Collins, CO 80521, USA

4 <sup>3</sup>Institute of Applied Ecology, Chinese Academy of Sciences, Shengyang 110016, China

5 *Correspondence to:* Xiaochun Wang ([wangx@nefu.edu.cn](mailto:wangx@nefu.edu.cn))

6 **Abstract.** We present a 260-year annual PDSI reconstruction based on a regional tree-ring width chronology of Scots  
7 pine (*Pinus sylvestris* var. *mongolica*) from four sample sites in the Daxing'an Mountains, northeast China. The model  
8 explained 38.2 % of the variance of annual PDSI during the calibration period from 1911 to 2010. Compared with local  
9 historical documents, nearby forest fire history data and hydroclimate reconstructions, our reconstruction is accurate  
10 and representative, and recorded the same dry years/periods. The drought of 1920s-1930s was more severe in the  
11 Daxing'an Mountains than in surrounding areas. A moisture increase caused by a recent rapid warming (warm-wet  
12 pattern) was identified for the Daxing'an Mountains, while a warm-dry pattern was found for the West-Central  
13 Mongolian Plateaus (mild drier) and their transition zones: the East Mongolian Plateaus (severe drier). Overall, the  
14 dry/wet variability of the Daxing'an Mountains and its relationship with the surrounding areas might be driven by  
15 Pacific and Atlantic Ocean oscillations (e.g., ENSO, PDO, AMO, NAO and SNAO) that influence the Asian monsoon,  
16 and in turn the local temperature and precipitation that influences regional drought. However, the Monsoon Asia  
17 Drought Atlas of "Cook" might inaccurately portray dry/wet variations in the Daxing'an Mountains.

18 **Keywords:** Drought reconstruction, Daxing'an Mountain, Tree rings, *Pinus sylvestris*, PDO and AMO, PDSI

## 19 1 Introduction

20 Drought as an important climate driver that is occurring more frequently with climate change and is a focus of scientific  
21 efforts around the world (Bao et al. 2015; Cook et al. 2010; Dai 2011, 2013; Davi et al. 2006; Li et al. 2016). Severe  
22 droughts can threaten agriculture and social activities, and also has a devastating impact on human lives and the survival  
23 of native and domestic plants and animals (Bao et al. 2015; Cook et al. 2010; Dong et al. 2013; Shen 2008; Sun 2007).  
24 Drought is one of the most severe and frequent natural disasters in China, especially in semi-arid and arid regions (Bao  
25 et al. 2015; Chen et al. 2015; Cook et al. 2010; Dong et al. 2013; Liang et al. 2006; Shen 2008; Sun and Liu 2013; Xu



26 1998). For instance, the 1920s severe drought affected all of northern China with significant economic losses to society  
27 and the economy (Dong et al. 2013; Liang et al. 2006; Shen 2008; Sun 2007). Natural droughts are preserved in the  
28 rings of trees in arid or semi-arid regions (Bao et al. 2015; Chen et al. 2015; Liang et al. 2006; Sun and Liu 2013; Wang  
29 and Song 2011). Recent studies indicate a trend of increasing drought frequency, persistence and severity due to global  
30 warming in many regions of the world (Bao et al. 2015; Cook et al. 2010; Dai 2011, 2013; Schrier et al. 2013). A rapid  
31 and pronounced warming accompanied by a decrease in precipitation has occurred in China, especially in high latitude  
32 and high altitude regions (Bao et al. 2015; Chen et al. 2015; Cook et al. 2010; Dai 2013; Sun and Liu 2013; Zhu et al.  
33 2017), producing severe and prolonged drought in recent decades, for example from 1999 to 2002 (Bao et al. 2015; Liu  
34 et al. 2009; Shen 2008).

35 The Daxing'an Mountains in northeast China is the transition zone from semiarid climate in the east to more arid  
36 conditions in the west, and monsoon driven precipitation in the south to a non-monsoon climate in the north (Bao et al.  
37 2015; Zhao et al. 2002). The Asian monsoon system has a direct impact on the occurrence, intensity and severity of  
38 droughts and floods (Bao et al. 2015; Cook et al. 2010; Liang et al. 2006; Wang et al. 2013; Wang et al. 2005; Zhao et  
39 al. 2002) that can have devastating effects on human society and economy as well as natural ecosystems (Sun 2007;  
40 Xu 1998). For instance, the drought of 2009 affected all of northeast China, with limited irrigation water available to  
41 more than 720,000 hectares of farmland, or drinking water for 81 million people  
42 ([http://www.chinadaily.com.cn/cndy/2009-08/13/content\\_8562996.htm](http://www.chinadaily.com.cn/cndy/2009-08/13/content_8562996.htm)). In addition, drought affected regions had a  
43 higher risk of forest fires in spring and summer (Sun 2007). Drought can facilitate the occurrence of large wildfires.  
44 For example, the Heilongjiang River fire in May 1987 killed over 200 people and burned ~73,000 km<sup>2</sup> (Sun 2007; Yao  
45 et al. 2017).

46 To better characterize current and future drought it is important to understand past drought patterns and their potential  
47 forcing mechanisms. However, the required meteorological records for the Daxing'an Mountains in northeast China  
48 only began in the 1950s. Therefore, tree rings can provide an important high resolution proxy for long-term drought  
49 reconstructions (Cook et al. 2010; Dai 2011; Pederson et al. 2013), although few studies have been conducted in north  
50 China, especially for hydroclimate reconstructions (Bao et al. 2015; Lv and Wang 2014; Wang and Lv 2012). Cook et  
51 al. (2010) reconstructed June–July–August Dai-PDSI for 534 grid points (Monsoon Asia Drought Atlas, MADA) in  
52 monsoon influenced Asia using a chronology developed from 327 tree-ring series. However, recent studies show that  
53 there has been some divergence of tree-ring-based drought reconstruction between the MADA and the individual  
54 sampling site or instrumental drought data, which might be caused by an insufficient spatiotemporal distribution of the  
55 tree-ring network used by MADA, especially in eastern Asia (Li et al. 2015; Liu et al. 2016). Additional reconstructions  
56 for eastern Asia are needed to gain a more thorough understanding of the Asian Monsoon climate variability. Many



57 researchers have used the Palmer drought severity index (PDSI), calculated from a water balance equation,  
58 incorporating air temperature and precipitation, to estimate drought periodicity and intensity (Bao et al. 2015; Cook et  
59 al. 2010; Dai 2011; Sun and Liu 2013). Here, we present a 260-year reconstruction of annual PDSI using tree ring  
60 chronologies from the Daxing'an Mountains to identify the timing of droughts and their correlation with eastern  
61 Mongolian Plateaus climate as well as their potential forcing mechanisms.

## 62 **2 Study area and climate**

63 The Daxing'an Mountains, in northeast Inner Mongolia and north-western Heilongjiang Province, form an important  
64 natural geographic divide between the Pacific Ocean and the north-western arid inland (Fig. 1). It is known to be a  
65 transition zone between regions with semiarid and arid, and monsoon and non-monsoon driven climates (Zhao et al.  
66 2002). The summer monsoons from the south-east are blocked by these mountains and cannot penetrating farther to  
67 the northwest. The western region is most arid, while farther east the climate is more humid and the slopes are forested.  
68 Summer weather is characterized by periodic incursions of warm, humid air masses from low-latitude oceans. During  
69 the winter, dry and cold air persists air masses invade from high latitudes.

70 This study was conducted in the high-latitude forested portion of the Daxing'an Mountains. The forests are dominated  
71 by Dahurian larch (*Larix gmelinii* Rupr.) and Scots pine (*Pinus sylvestris* L. var. *mongolica* Litv.). Soils are  
72 predominantly brown coniferous and dark-brown forest peat (Xu 1998). Meteorological data from stations nearest to  
73 our sample sites (Xiaoergou station; Table 1) have an annual mean temperature range from  $-2.6$  to  $2.0$  °C. The extreme  
74 coldest and hottest months are January ( $-39.5$  °C) and June ( $32.8$  °C). Annual precipitation ranges from 289 to 1000  
75 mm (averaging 500 mm) with high interannual variations. Rain during June to August accounts for 68% of total annual  
76 precipitation (Fig. 2). Low relative humidity occurs in all months outside of the growing season. Severe drought occurs  
77 frequently, especially in spring and summer (Sun 2007), and produces high fire risk. This region has the highest average  
78 annual burned area in China (Sun 2007).

### 79 **2.1 Tree-ring data**

80 Trees were sampled from four little-disturbed Mongolian pine-dominated sites in centre Daxing'an Mountains in May  
81 2011 and 2012 (Table 1; Fig. 1). The sites are separated by more than 100 km (Figure 1). One core was obtained at  
82 breast height from 120 living old trees using a 5.15-mm-diameter increment borer (500 mm length, two screws, Haglöf  
83 Sweden, Längsele, Sweden) (see Table 2 for detailed information). Each sample tree was selected to avoid the influence  
84 of identifiable stand disturbances (including animal and human disturbance, windstorm, snow and fire damage) and  
85 any obvious abnormal growth. All cores were dried, mounted, surfaced, and cross-dated following standard techniques



86 of dendrochronology (Cook and Kairiukstis 1990; Fritts 1976). Ring widths were measured with a precision of 0.001  
87 mm using a Velmex measuring system (Velmex, Inc., Bloomfield, NY, USA).

88 The quality of cross-dating and measurement was evaluated using the COFECHA program (Holmes 1983). Two cores,  
89 that were weakly correlated with the master chronology were excluded from further analysis. Successively, the age-  
90 related trends were removed by fitting a cubic smoothing spline with a 50% frequency response cut-off at 2/3 of the  
91 series length using the ARSTAN program (Cook and Kairiukstis 1990). Tree-ring indices were calculated as ratios  
92 from the estimated growth curves. Autocorrelation was removed by autoregressive modelling, and site chronologies  
93 were calculated using a bi-weighted robust mean (Cook and Kairiukstis 1990). Standard dendrochronological statistics  
94 were computed to evaluate the quality of chronologies between tree mean correlation (Rbt) (Cook and Kairiukstis 1990)  
95 and ring mean sensitivity (Fritts 1976) (Table 3). The four chronologies have high values in standard deviation, mean  
96 sensitivity, mean series correlation and agreement within population. The chronologies reflect high inter-annual  
97 variation and a strong common signal and are excellent proxies for regional climate. Since all four chronologies agree  
98 well (Table 3), we merged all samples to develop a single robust regional chronology. Running RBAR (mean  
99 correlation between series) and EPS (expressed population signal) statistics were calculated for 51-year intervals of the  
100 chronology with 25-year overlaps to assess confidence in the chronology. RBAR averages variance among ring width  
101 series in a chronology, which estimates chronology signal strength (Cook and Kairiukstis 1990). EPS estimates the  
102 degree to which the chronology represents a hypothetical chronology based on a finite number of trees that match a  
103 hypothetically perfect chronology; EPS values greater than 0.85 are generally considered to be an acceptable threshold  
104 for a reliable chronology (Wigley et al. 1984). The regional chronology spanned the period from 1725 to 2010, and the  
105 reliable interval (EPS > 0.85) was 1751-2010 corresponding to eight cores/trees.

## 106 **2.2 Climate and statistical analyses**

107 Climate data were obtained from the China Meteorological Data Sharing Servicing System. The closest weather station  
108 to the sample sites is Xiaogou (Table 1), about 70-91 km away. Large-scale climate data (e.g. Atlantic Multidecadal  
109 Oscillation, AMO; Pacific Decadal Oscillation, PDO; North Atlantic Oscillation, NAO) and high-resolution gridded  
110 climate data (Table 1; e.g. gridded temperature, precipitation and drought indices) were downloaded from the website:  
111 <http://climexp.knmi.nl/>. Pearson correlation analysis was employed to determine climate–tree growth relationships.  
112 The gridded climate dataset is much longer and has high homogeneity and coherency with instrumental records (Fig.  
113 2), the gridded monthly total precipitation (CRU GPCC; Schneider et al. (2015)) and mean temperature (CRU TS3.23;  
114 Jones and Harris (2013)) nearest to our sites were used for climate response analyses. Besides, the nearby gridded  
115 monthly Palmer Drought Severity Index (PDSI) data from Dai (2011) (Dai-PDSI, hereafter), a most commonly used



116 drought index, was used to assess the effects of drought. Correlation analyses between the regional chronology and  
117 monthly climatic records were calculated from the previous July to the current July.

118 A linear regression model was used to develop the drought reconstruction, and a traditional split-period calibration  
119 verification method was applied to examine model fit (Fritts 1976). Statistical parameters included the  $R^2$ , Sign test  
120 (ST), reduction of error (RE), coefficient of efficiency (CE), product means test (PMT) and root mean square error  
121 (RMSE) (Cook and Kairiukstis 1990; Fritts 1976). Spatial correlation of measured and reconstructed drought variables  
122 with regional gridded CRU-PDSI (Schrier et al. 2013) were performed to examine the spatial representativeness of our  
123 reconstruction using the KNMI climate explorer. We also carried out the superposed epoch analysis (SEA) between  
124 nearby forest fire history and drought variables to further validate the accuracy of our reconstruction, since seasonal or  
125 annual droughts are usually a key factor in forest fire severity in the Daxing'an Mountains (Shen 2008; Sun 2007). Two  
126 regional forest fire event lists (Mengkeshan and Pangu; Fig. 1) reconstructed by tree-ring scars in nearby forest were  
127 used (Yao et al. 2017) and the SEA were carried out using software FHAES V2.0.0 (<https://www.frames.gov/partner-sites/fhaes/download-fhaes/>). In addition, the consistency between our reconstruction and other local drought related  
128 time series including the gridded Standardised Precipitation-Evapotranspiration Index (SPEI), the Monsoon Asia  
129 Drought Atlas (MADA) from Cook et al. (2010) (Cook-PDSI, hereafter) and Self-calibrating PDSI from Schrier et al.  
130 (2013) (scPDSI, hereafter), and nearby tree-ring-based hydroclimatic reconstructions (the December–March  
131 precipitation reconstruction of the A'li River (AR) in the Daxing'an Mountain from Lv and Wang (2014), the April–  
132 August SPEI reconstruction of the Hulun Buir steppe (HB) on the east edge of Mongolian Plateaus from the western  
133 Daxing'an Mountains (Bao et al. 2015), and the tree-ring-based streamflow reconstruction of Selenge River (SR) from  
134 Davi et al. (2006) in the Mongolian Plateaus, Mongolia) were evaluated and described by filtering and moving  
135 correlations. To identify spatialtemporal patterns of drought in Northeast Asia and their relationship with our  
136 reconstructed drought history, we further analyzed correlations with four other hydroclimatic reconstructions from the  
137 Daxing'an Mountains and the Mongolian Plateaus (Fig. 1). To make the comparison better visualized, all above series  
138 were standardized using Z-scores and then smoothed with a 21-year moving averaged to highlight low-frequency  
139 drought signals.  
140

141 To evaluate the extreme dry and wet years in the historical period, we defined extremely dry and wet years with the  
142 annual PDSI value being lower or higher than the average  $\pm 1.5$  SD. We assessed the multiyear dry/wet periods based  
143 on the intensity (average departure values from the long-term mean) and magnitude (cumulative departure values from  
144 the long-term mean). A spectral analysis were applied to identify the periodicity of dry/wet variability and possible  
145 effects of large-scale climate using Multi-taper method (MTM) program (Mann and Lees 1996). To further confirm  
146 the linkage between large-scale climate and regional drought, we analysed their relationship with Pearson correlation



147 analysis. Teleconnections between reconstructed drought variables and global sea surface temperature ( $0.5^{\circ} \times 0.5^{\circ}$ ) were  
148 carried out to verify the potential drivers of large-scale climate on local drought.

### 149 **3 Results**

#### 150 **3.1 Tree growth–climate relationships**

151 The radial growth of Scots pine was significantly ( $p < 0.05$ ) positively correlated with precipitation in all months except  
152 the previous November and current February (Fig. 4a). Temperature of the previous November to current May (except  
153 for current April) was significantly correlated with ring widths at the 95% confidence level (Fig. 4a). The highest  
154 positive Pearson's correlation coefficients were found between the ring width Scots pine chronology and monthly total  
155 precipitation of October ( $r = 0.35$ ,  $p < 0.05$ ) and previous December temperature ( $r = 0.35$ ,  $p < 0.05$ ). Radial growth of  
156 Scots pine in the Daxing'an Mountains was influenced by both precipitation and temperature, but the effects of  
157 precipitation were stronger, which revealed annual precipitation sensitivity of the Scots pine chronology during the last  
158 century (Fig. 4a). Furthermore, we calculated the correlation between the tree-ring index and Dai-PDSI (common  
159 period of 1901-2010), which takes into account temperature and precipitation (Dai 2011). Significant ( $p < 0.05$ ) positive  
160 correlations between tree rings and PDSI was found for all months from the previous July to the current July (Fig. 4b).  
161 The correlation between tree growth and annual (Jan-Dec) average PDSI had the highest correlation ( $r = 0.62$ ,  $p <$   
162  $0.0001$ ,  $n = 110$ ) between tree growth and PDSI data among the annual, seasonal or individual month scales. The results  
163 confirmed that water conditions had a significant controlling influence on Scots pine growth over a last century (Fig.  
164 6).

#### 165 **3.2 PDSI reconstruction**

166 The regression model between the tree-ring indices (predictors) and annual PDSI (predicted) for the calibration period  
167 was as follows:

$$168 \quad D_t = 6.69 I_t - 7.13, (R = 0.62, N = 100, F = 60.52, p < 0.0001) \quad (1)$$

169 where  $D_t$  is the annual PDSI and  $I_t$  is the tree-ring index at year  $t$ . For the calibration period 1911–2010, the  
170 reconstruction explained 38.2% of the PDSI variation (37.6% after accounting for the loss of degrees of freedom). As  
171 shown in Figure 5a, the actual and estimated annual PDSI of Daxing'an Mountain have similar trends and are parallel  
172 to each other during the calibration period. However, the estimated PDSI did not capture the magnitude of extreme dry  
173 or wet conditions. Spatial correlation analysis show that the actual and estimated PDSI had a strong and similar spatial  
174 correlation pattern with the Northeast Asia grided scPDSI ( $0.5^{\circ} \times 0.5^{\circ}$ ) (Fig. 6).



175 The split calibration-verification test showed that the explained variances were high during the two calibration periods  
176 and the statistics of  $R$ ,  $R^2$ , ST, PMT are all significant at  $p < 0.05$ , which indicated that the model was reliable (Table  
177 4). The most rigorous tests, RE and CE, were also positive for both verification periods (Cook and Kairiukstis 1990;  
178 Fritts 1976) (Table 4).

### 179 **3.3 Drought-wet variations**

180 The reconstructed annual PDSI with 11-year moving average exhibited a mean of 0.48 and a standard deviation (SD)  
181 of  $\pm 1.15$  during the past 260 years (Fig. 5b). Reconstruction of the annual PDSI displayed strong interannual to decadal  
182 scale variability throughout the period 1751 to 2010. During the last 260 years, there were 22 extreme dry years  
183 (accounting for 8.5%) and 15 extreme wet years (5.8%) (Table 5). Most extreme dry years occurred in the 19<sup>th</sup> (12  
184 years, accounting for 48%) and 20<sup>th</sup> (9 years, accounting for 36%) centuries, and a majority of extreme wet years  
185 occurred in the 20<sup>th</sup> century (9 years, accounting for 60%). Among the extreme years, 1784, 1853, 1818, 1862 and 1863  
186 were the five driest years, and 1998, 1952, 1770, 1993 and 1766 were the five wettest years (Table 5). We also found  
187 that many extreme dry or wet years occurred in succession.

188 Compared with the severe single-year droughts, multi-year droughts had the greatest effect on tree growth, and we  
189 further defined the dry and wet periods as those when the 11-year moving average PDSI was more than 0.5 SD from  
190 the mean for at least 2 consecutive years. Four dry periods, AD 1751–1752, 1812–1817, 1847–1866 and 1908–1927,  
191 and four wet periods 1757–1771, 1881–1902, 1952–1955 and 1989–2004 were identified (Table 5). The dry periods of  
192 1847–1866 and 1906–1927 were the longest, spanning 20 years, while the longest wet period, from 1881–1902, lasted  
193 for 22 years (Table 5). The multiyear drought of 1847–1866 was the most serious due to long duration and intensity,  
194 and 1906–1927 was the second most significant drought (Table 6). Wet periods of 1757–1771 and 1989–2004 were the  
195 most remarkable in terms of intensity and duration (Table 6).

196 Spectral analysis revealed that the dry and wet variations in the Daxing'an Mountain climate had some significant (95%  
197 or 99% confidence level) periodicities at 46.5–78.7 (99%), 12.05–12.33, 5.75–5.82 (99%), 4.95–5.02, 4.78–4.83, 3.32  
198 (99%), 2.92, 2.44–2.5, 2.26–2.32 (99%), 2.09–2.15 (99%) and 2.01–2.02 (99%) years, which corresponded to significant  
199 cycle peaks present in Figure 7.

## 200 **4 Discussion**

### 201 **4.1 Climate-growth relationship**

202 Scots pine is an extremely drought-tolerant species and drought stress is thought to be the main climate limitation for  
203 its radial growth in semi-arid or arid regions, such as in the Mongolia Plateaus and western Daxing'an Mountains (Bao



204 et al. 2015; Davi et al. 2006; Liu et al. 2009; Pederson et al. 2013). Previous dendroclimatic studies from these regions  
205 suggest that radial growth of Scots pine is sensitive to humidity, precipitation or drought (e.g. PDSI, SPEI), and most  
206 analyses have reconstructed hydroclimatic history (Bao et al. 2015; Liu et al. 2009). In these areas, the radial growth  
207 of Scots pine usually has a typical climatic (drought) response pattern with positive tree growth response to increasing  
208 precipitation and negative response to increasing temperature (Bao et al. 2015; Davi et al. 2006; Liu et al. 2009). This  
209 typical drought response pattern usually is found in other drought or wetness tree ring reconstructions (Li et al. 2016;  
210 Liu et al. 2016). In this study, the correlation between tree-ring indices and monthly precipitation and temperature data  
211 revealed that the radial growth of Scots pine was mainly limited by water, which is consistent with the physiological  
212 characteristics of tree species living in arid regions. A significant positive relationship between the tree-ring index and  
213 PDSI in all months supported moisture as the main limiting factor for radial growth of Scots pine (Fig. 4b).

214 A drought response was also found in Dahurian larch (Wang and Lv 2012), another important conifer tree species in  
215 the study area. However, the typical drought response to temperature was not obvious, and the radial growth of Scots  
216 pine was not significantly negatively correlated with growing season (July-September) temperature (Fig. 4a). On the  
217 contrary, a significant positive response of radial growth to winter (non-growing season) temperature was found,  
218 suggesting that higher winter and spring temperatures prolong the growth period and increased nutrient availability for  
219 trees during the summer (Hollesen et al. 2015; Zhu et al. 2017). This phenomenon might be due to the relatively humid  
220 climate and the northern latitude of our study sites, where the positive effect of temperature was greater than the  
221 negative effect resulting from drought stress (Wang and Song 2011). Similar drought response patterns were also found  
222 in tree-ring-based drought reconstructions in the middle Qilian Mountains (Sun and Liu 2013) and the Tianshan  
223 Mountains of western China (Chen et al. 2015).

#### 224 **4.2 Comparison with regional record**

225 We used local historical records to verify our PDSI reconstruction for the timing of extreme dry years or periods.  
226 During the last 260 years, 60.1% (13/22) of extreme dry years were noted in historical documents (Shen 2008; Sun  
227 2007). Tree rings can not fully record the continuous drought events (years) resulting in a limited percentage or  
228 correspondence. For example, the extreme drought years of 1860-1865 were recorded only during 1861 in our  
229 reconstruction. Thus, some severe drought events affect radial tree growth in some but not all years (Fritts 1976).  
230 Besides, the lag response of radial growth to climate (drought) might have a great contribution to unrecorded extreme  
231 drought events (Fritts 1976), for instance local historical documents record the dry years of 1817 and 1855 and these  
232 appear narrower rings in that year, or as an extreme dry event in the following year. Two multiyear droughts recorded  
233 in tree-rings, 1847–1866 and 1908–1927, can both be identified in historical documents (Shen 2008; Sun 2007).  
234 Moreover, SEA between forest fire history and reconstructed drought variables revealed that a significant drop of PDSI



235 values occurred during the year of the forest fire in Mengkeshan and Pangu (Fig. 8), further validating the accuracy of  
236 our reconstruction. Spatial correlation analysis indicated a strong correlation pattern between our reconstruction and  
237 gridded scPDSI in Northeast Asia (Fig. 9), and our reconstruction also represents drought/wet variations in surrounding  
238 geographic regions. During the common periods, our reconstruction shares a similar dry/wet fluctuation with the  
239 precipitation of A'li River and SPEI of Hulun Buir steppe both in the low and high frequency (Fig. 9b-d). Significant  
240 ( $p < 0.05$ ) correlations among them were found in low and high frequency and some common dry/wet periods were  
241 highlighted in Figure 9, which confirmed that our drought reconstruction could almost fully account for the dry/wet  
242 variations of the Daxing'an Mountains, northeast China.

243 It's important to note that our drought reconstruction and the MADA of "Cook" from the same PDSI grid was not  
244 consistent and showed a completely opposite trend ( $R_L = -0.19^{**}$ ;  $p < 0.01$ ) in low frequency (Fig. 9). Negative  
245 correlations between the MADA and the SPEI ( $R_L = -0.311^{**}$ ;  $p = 0.03$ ) and scPDSI ( $R_L = -0.126$ ;  $p = 0.236$ ), positive  
246 correlations between our drought reconstruction and the SPEI ( $R_L = 0.950^{**}$ ;  $p < 0.01$ ) and scPDSI ( $R_L = 0.807^{**}$ ;  $p$   
247  $< 0.01$ ) were also found, although it has a seasonal difference with our drought reconstruction. These both imply that  
248 MADA of "Cook" might be inaccurate or even reversed in characterizing dry/wet variations in the Daxing'an  
249 Mountains. Similar divergence of tree-ring-based drought reconstruction between the MADA and individual sampling  
250 sites was also found by Li et al. (2015) from Guancen Mountain and Liu et al. (2016) from central Inner Mongolia. The  
251 insufficient spatiotemporal distribution of tree-ring network, especially in eastern China, used by MADA might be the  
252 main reason for this divergence/inaccuracy (Cook et al. 2010; Li et al. 2015; Liu et al. 2016). Therefore, our drought  
253 reconstruction is necessary to gain a thorough understanding of the East Asian Monsoon climate variability.

254 In a larger spatial scale, the streamflow reconstruction of Selenge River in the West-Central Mongolian Plateaus from  
255 Davi et al. (2006) presented a significant positive correlation with our drought reconstruction in low frequency ( $R_L =$   
256  $0.29^{**}$ ;  $p < 0.01$ ) during the full periods. Our reconstructed PDSI also displayed some common variation trends or  
257 dry/wet periods with the reconstructed streamflow variations from the Selenge River (Davi et al. 2006), especially in  
258 the decadal scale. These relationships suggest that there are common drivers affecting the dry/wet variations of the  
259 Daxing'an Mountains and the West-Central Mongolian Plateau, although there might be some discordance. Among  
260 those differences, the most obvious is the completely different dry/wet variation trends among the Daxing'an Mountains  
261 (wetter), the West-Central Mongolian Plateaus (mild drier) as well as their transition zones: The East Mongolian  
262 Plateaus (Hulun Buir steppe; drier) since the late 1970s (Fig. 10a). Similar results were also found by Dai (2013), who  
263 presented a different dry-wet pattern under global warming using observations and models. In the Tibetan Plateau, Li  
264 et al. (2016) found moisture increase coherent to rapid warming (warm-wet). Although the reason for this divergence  
265 needs to be further studied, it might be related to the different response to the phase shift (negative to positive) of the



266 Pacific Decadal Oscillation (PDO) in 1976 and 1977 (Ma 2007; Wang et al. 2014). Ma (2007) found that the positive  
267 phase of PDO usually corresponds to the drought period with warming and less precipitation, while the negative PDO  
268 phase often matches the wet period with low temperature and more precipitation. Besides, the drought trend caused by  
269 the persistent significant warming in semi-arid or arid regions might be more serious than in semi-humid or humid  
270 regions (Dai 2013). In addition, a different record of severe drought that occurred over a large geographic area of  
271 northern Asia during the 1920s to 1930s, has been reported by many other studies in north China (Bao et al. 2015; Chen  
272 et al. 2015; Liang et al. 2006; Liu et al. 2009). As indicated by the tree-ring series, the drought event of 1920s-1930s  
273 in the Daxing'an Mountains is more severe than in the transitional East Mongolian Plateaus (the Hulun Buir steppe),  
274 which was consistent with the result of Dong et al. (2013). The drought, however, was not found in the West-Central  
275 Mongolian plateaus (the Selenge River). On the contrary it was very moist in that time (Fig. 10). Different spatial  
276 patterns of severe drought over the northeast Asian might be associated with the intensity and scope of the strong El  
277 Niño-Southern Oscillation (ENSO) during this period (Dong et al. 2013).

#### 278 **4.3 Linkages to the Pacific and Atlantic Oceans**

279 Spectral analysis revealed that some significant cycles exist in our drought reconstruction (Fig. 7). Among them, are  
280 significant high-frequency 2.0 - 5.8-year periodicities within the 2-7 year cycles of ENSO (Li et al. 2013), and we have  
281 shown that the dry/wet variations in the Daxing'an Mountain might be related to ENSO. Similarly, local dry-wet  
282 changes driven by large-scale climate oscillation of the ENSO occur in tree-ring-based hydroclimatic reconstructions,  
283 such in northeast China (Bao et al. 2015; Lv and Wang 2014; Wang and Lv 2012), northwest China (Chen et al. 2015;  
284 Sun and Liu 2013) and the Mongolian Plateaus (Davi et al. 2006). Strong connection appears between our  
285 reconstruction and annual SSTs over the Pacific Ocean, especially nearby the equator, the north Pacific, as well as the  
286 east and west coasts of the Pacific Ocean (Fig. 11). We also calculated the correlation between the Niño 3 index and  
287 the dry-wet index (averaged Z-scores) of the Daxing'an Mountains and show a significant positive correlation exists  
288 between them in both low and high frequencies (Table 7, Fig. 10b). These results reveal the potential links between  
289 ENSO and dry/wet variations of the Daxing'an Mountains, Northeast China. Although the mechanisms need to be  
290 further studied, the close relationship between the oscillatory changes of North Atlantic SST and the Asian monsoon  
291 have been demonstrated. ENSO might indirectly influence the dry-wet change of the Daxing'an Mountains by affecting  
292 the local climate (Shuai et al. 2016). Wang et al. (2013) found that the ENSO could potentially drive or affect the Asian  
293 monsoon, which in turn affects temperature and precipitation to drive local drought variations, as a possible driving  
294 mechanism (Fig. 12). Significant positive correlations between the Niño 3 index and local climate (temperature and  
295 precipitation) further confirms our inference (Table 7).



296 The 12.05-12.33-year cycles were close to the 10- to 12-year activity cycle indicating that dry/wet variations in the  
297 Daxing'an Mountains might be controlled by solar activity (Shindell et al. 1999). Many previous studies have  
298 demonstrated that solar activity can drive local dry-wet variations (Chen et al. 2015; Hodell et al. 2001; Sun and Liu  
299 2013). In northeastern China, Hong et al. (2001) also found the signals of solar activity in a 6000-year record of drought  
300 and precipitation. Significant positive correlations between the Total Solar Irradiance (TSI; reconstruction from IPCC  
301 AR5) and the dry-wet index (averaged Z-scores) of the Daxing'an Mountains both in low and high frequencies, and  
302 between the TSI and local climate (temperature and precipitation) further confirmed the relationship between solar  
303 activity and local drought (Table 7, Fig. 10b). Wang et al. (2005) found a potential link between the Asian monsoon  
304 and solar changes. Local drought variations of the Daxing'an Mountains might be driven by solar activity that affects  
305 the Asian monsoon and influences local climate (temperature and precipitation) (Fig. 12).

306 Cycles of 46.5 - 48.8 years might be related to the Pacific Decadal Oscillation (PDO), since it coincided with the 50-  
307 70 year cycle of PDO (Macdonald and Case 2005). This was verified by the strong connection between our drought  
308 reconstruction and annual SSTs over the Pacific Ocean (Fig. 11). The cycles/signals of PDO widely exist in most tree-  
309 ring-based drought reconstructions (Bao et al. 2015; Chen et al. 2015; Sun and Liu 2013; Wang and Lv 2012), and  
310 many studies have confirmed that PDO can influence drought conditions in China (Bao et al. 2015; Cook et al. 2010;  
311 Ma 2007). The potential linkages between the PDO and local drought in the Daxing'an Mountains is further confirmed  
312 by the significant positive correlations between the PDO index (Mann and Lees 1996) and the dry-wet index of the  
313 Daxing'an Mountains both in low and high frequencies (Table 7, Fig. 10b). The positive/warm phase of the PDO index  
314 usually corresponds with drought periods, and the PDO negative/cold phase often matches wet periods (Ma 2007). For  
315 example, the severe drought of the 1920s - 1930s corresponds to the PDO negative phase. The PDO might drive the  
316 dry/wet variations of the Daxing'an Mountains by modifying the intensity or location of Asia Monsoon (Bao et al. 2015;  
317 Cook et al. 2010; Ma 2007). Significant positive correlations between the PDO index and local climate (temperature  
318 and precipitation) were also found, revealing that the PDO may affect the dry/wet variations of the Daxing'an Mountains  
319 by regulating the Asian monsoon to affect local temperature or precipitation (Fig. 12). Similar results were found in a  
320 nearby tree-ring-based drought reconstruction ((Bao et al. 2015).

321 Ultimately, the cycles around 73-years might result from oscillatory changes in the North Atlantic SST, which has a  
322 period of 60–90 years (Knudsen et al. 2011). Spatial correlations between our drought reconstruction and annual SSTs  
323 also show a strong teleconnection over the Atlantic Ocean (Fig. 11), which further confirmed potential linkages between  
324 the North Atlantic SSTs and dry-wet cycles in the Daxing'an Mountains. Although our study area is far away from the  
325 Atlantic Ocean, many studies have confirmed that large-scale climate oscillations in the Atlantic Ocean (such as the  
326 Atlantic Multidecadal Oscillation (AMO), North Atlantic Oscillation (NAO) as well as Summer NAO (SNAO)) could



327 affect the local climate or tree growth in China (Bates 2007; Linderholm et al. 2011; Linderholm et al. 2013; Sun et al.  
328 2008; Wang et al. 2011). Most dendroclimatological studies on drought reconstruction also found cycles/signals of  
329 oscillatory changes correlated with North Atlantic SSTs (e.g. AMO, NAO and SNAO), including in the Daxing'an  
330 Mountains (Lv and Wang 2014; Wang and Lv 2012), eastern Mongolian Plateaus (Bao et al. 2015; Liu et al. 2009),  
331 West-Central Mongolia (Davi et al. 2006), and northwest China (Chen et al. 2015; Sun and Liu 2013). Furthermore, we  
332 also identified significant negative/postive correlation between the dry-wet change of the Daxing'an Mountains (Z-  
333 score) and the AMO, NAO and SNAO index both in low or high frequency (Table 7, Fig. 10c). The strong AMO signal  
334 (Wang et al. 2011) and teleconnections with SNAO (Linderholm et al. 2013) also have been found in tree-ring widths  
335 of Scots pine in northeast China and eastcentral Siberia during the last 400 years. All of these studies confirmed that  
336 oscillatory changes of the North Atlantic SST (e.g. AMO, NAO and SNAO) could drive dry-wet changes in the  
337 Daxing'an Mountains. Although its mechanism needs to be further studied, the close relationship between the  
338 oscillatory changes of North Atlantic SST and the Asian monsoon has been demonstrated. Recent studies have shown  
339 that the AMO (Wang et al. 2013), NAO (Feng and Hu 2008) and SNAO (Linderholm et al. 2011) all have the potential  
340 to drive or affect the Asian monsoon. In this study, although only the AMO index was significantly correlated with  
341 local climate (temperature and precipitation) (Table 7, Fig. 10c), it also confirmed that the oscillatory changes of North  
342 Atlantic SST, especially the AMO, could drive wet-dry changes in the Daxing'an Mountains by influencing the Asia  
343 Monsoon (local temperature and precipitation, Fig. 12) (Bao et al. 2015; Chen et al. 2015; Cook et al. 2010; Li et al.  
344 2015; Linderholm et al. 2011; Sun et al. 2008).

## 345 **5 Conclusion**

346 In this study, we developed a 260 years (1751 to 2010) tree-ring chronology for Scots pine (*Pinus sylvestris* L. var.  
347 *mongolica* Litv.) from four sample sites of the Daxing'an Mountains, in northeast China. Using a significant correlation  
348 between the tree-ring index and annual Dai-PDSI ( $R = 0.62$ ,  $p < 0.01$ ), we reconstructed a new annual PDSI record for  
349 the Daxing'an Mountain that explains 38.2 % of the PDSI variance during the period 1911–2010. Four dry and wet  
350 periods were found during the past 260 years. The extreme dry years in our reconstruction are consistent with local  
351 historical records and nearby forest fire history. Results show that our reconstruction not only accounted for the dry  
352 and wet variations for the Daxing'an Mountains, but also are representative of the West-Central Mongolian Plateaus,  
353 especially at the decadal scale. Drought of 1920s-1930s in the Daxing'an Mountains was more severe than in  
354 surrounding areas. Moreover, there has been obvious warming and wetting since the late 1970s, which is distinct from  
355 events that occurred on the Mongolian Plateaus, especially in its transition zones. The MADA of "Cook" might be  
356 inaccurate or even reversed in referring to the dry/wet variations in the Daxing'an Mountains, which might be due to  
357 insufficient spatiotemporal distribution of the tree-ring network in eastern China. Overall, the dry/wet variability of the



358 Daxing'an Mountains and its relationship with the surrounding areas might be driven by oscillations of the Pacific and  
359 Atlantic Oceans (e.g., ENSO, PDO, AMO, NAO and SNAO). Those large-scale climate oscillations controls the Asian  
360 monsoon, which in turn affects temperature and precipitation to influence local drought variations.

361

### 362 **Author Contributions**

363 For this article, XW and SH initiated the study, LZ and QY performed field sampling and data preprocessing, LZ  
364 performed statistical analyses and wrote the manuscript, DC and SH wrote partial discussion and revised the whole  
365 manuscript, XW performed partial analyses and produced figures.

### 366 **Funding**

367 This work was supported by the Key Project of the China National Key Research and Development Program  
368 (2016YFA0600800), the National Natural Science Foundation of China (Nos. 41471168 and 31370463), the Program  
369 for Changjiang Scholars and Innovative Research Team in University (IRT-15R09), and the Fundamental Research  
370 Funds for the Central Universities (2572016AA32).

### 371 **Conflict of Interest Statement**

372 The authors declare that the research was conducted in the absence of any commercial or financial relationships that  
373 could be construed as a potential conflict of interest.

### 374 **Acknowledgements**

375 We thank Yongxian Lu and Lei Zhang of Northeast Forestry University for assistance in the field.

376

### 377 **References**

- 378 Bao G, Liu Y, Liu N, Linderholm HW (2015) Drought variability in eastern Mongolian Plateau and its linkages to the  
379 large-scale climate forcing. *Climate Dynamics* 44:717-733  
380 Bates GT (2007) Influence of the Atlantic multidecadal oscillation on the winter climate of East China. *Advances in*  
381 *Atmospheric Sciences* 24:126-135  
382 Chen F et al. (2015) Tree-ring recorded hydroclimatic change in Tianshan mountains during the past 500 years.  
383 *Quaternary International* 358:35-41



- 384 Cook ER, Kairiukstis LA (1990) Methods of dendrochronology: applications in the environmental sciences. Springer,  
385 Cook ER, Anchukaitis KJ, Buckley BM, D'Arrigo RD, Jacoby GC, Wright WE (2010) Asian monsoon failure and  
386 megadrought during the last millennium. *Science* 328:486-489
- 387 Dai A (2011) Characteristics and trends in various forms of the Palmer Drought Severity Index during 1900–2008.  
388 *Journal of Geophysical Research: Atmospheres* 116
- 389 Dai A (2013) Increasing drought under global warming in observations and models. *Nature Climate Change* 3:52-58
- 390 Davi N, Jacoby G, Curtis A, Baatarbileg N (2006) Extension of Drought Records for Central Asia Using Tree Rings:  
391 West-Central Mongolia. *Journal of Climate* 19:288-299
- 392 Dong A, Wang J, Li Y (2013) The Disaster and Causes of Serious Drought in Seven Provinces of Northern China in  
393 1920. *Journal of Arid Meteorology* 31:750-755
- 394 Feng S, Hu Q (2008) How the North Atlantic Multidecadal Oscillation may have influenced the Indian summer  
395 monsoon during the past two millennia. *Geophysical Research Letters* 35
- 396 Fritts HC (1976) Tree rings and climate. Elsevier, Amsterdam, Netherland
- 397 Hodell DA, Brenner M, Curtis JH, Guilderson T (2001) Solar forcing of drought frequency in the Maya lowlands.  
398 *Science* 292:1367-1370
- 399 Hollesen J, Buchwal A, Rachlewicz G, Hansen BU, Hansen MO, Stecher O, Bo E (2015) Winter warming as an  
400 important co-driver for Betulanana growth in western Greenland during the past century. *Global Change*  
401 *Biology* 21:2410–2423
- 402 Holmes RL (1983) Computer-assisted quality control in tree-ring dating and measurement. *Tree-ring bulletin* 43:69-  
403 78
- 404 Hong Y et al. (2001) A 6000-year record of changes in drought and precipitation in northeastern China based on a  $\delta$   
405  $^{13}\text{C}$  time series from peat cellulose. *Earth and Planetary Science Letters* 185:111-119
- 406 Jones P, Harris I (2013) CRU TS3. 20: Climatic Research Unit (CRU) Time-Series (TS) Version 3.20 of High  
407 Resolution Gridded Data of Month-by-Month Variation in Climate (January 1901–December 2011). NCAS  
408 British Atmospheric Data Centre
- 409 Knudsen MF, Seidenkrantz M-S, Jacobsen BH, Kuijpers A (2011) Tracking the Atlantic Multidecadal Oscillation  
410 through the last 8,000 years. *Nature Communications* 2:178
- 411 Li J et al. (2013) El Niño modulations over the past seven centuries. *Nature Climate Change* 3:822-826
- 412 Li J, Shi J, Zhang DD, Yang B, Fang K, Yue PH (2016) Moisture increase in response to high-altitude warming  
413 evidenced by tree-rings on the southeastern Tibetan Plateau. *Climate Dynamics*:1-12
- 414 Li Q, Liu Y, Song H, Yang Y, Zhao B (2015) Divergence of tree-ring-based drought reconstruction between the  
415 individual sampling site and the Monsoon Asia Drought Atlas: an example from Guancen Mountain. *Science*  
416 *Bulletin*:1688-1697
- 417 Liang E et al. (2006) The 1920S Drought Recorded by Tree Rings and Historical Documents in the Semi-Arid and  
418 Arid Areas of Northern China. *Climatic Change* 79:403-432
- 419 Linderholm HW et al. (2011) Interannual teleconnections between the summer North Atlantic Oscillation and the  
420 East Asian summer monsoon. *Journal of Geophysical Research: Atmospheres* 116
- 421 Linderholm HW et al. (2013) Exploring teleconnections between the summer NAO (SNAO) and climate in East Asia  
422 over the last four centuries—A tree-ring perspective. *Dendrochronologia* 31:297-310
- 423 Liu Y, Bao G, Song H, Cai Q, Sun J (2009) Precipitation reconstruction from Hailar pine (*Pinus sylvestris* var.  
424 *mongolica*) tree rings in the Hailar region, Inner Mongolia, China back to 1865 AD. *Palaeogeography,*  
425 *Palaeoclimatology, Palaeoecology* 282:81-87
- 426 Liu Y et al. (2016) Tree-ring-width-based PDSI reconstruction for central Inner Mongolia, China over the past 333  
427 years. *Climate Dynamics*:1-13
- 428 Lv S, Wang XC (2014) Growth-climate response and winter precipitation reconstruction of *Pinus sylvestris* var.  
429 *mongolicain* A'li River of Greater Khingan Range. *Journal of Northeast Normal University*
- 430 Ma Z (2007) The interdecadal trend and shift of dry/wet over the central part of North China and their relationship to  
431 the Pacific Decadal Oscillation (PDO). *Chinese Science Bulletin* 52:2130-2139
- 432 Macdonald GM, Case RA (2005) Variations in the Pacific Decadal Oscillation over the past millennium. *Geophysical*



- 433 Research Letters 32:93-114
- 434 Mann ME, Lees JM (1996) Robust estimation of background noise and signal detection in climatic time series.
- 435 Climatic change 33:409-445
- 436 Mann ME et al. (2009) Global signatures and dynamical origins of the Little Ice Age and Medieval Climate Anomaly.
- 437 Science 326:1256-1260
- 438 Pederson N et al. (2013) Three centuries of shifting hydroclimatic regimes across the Mongolian Breadbasket.
- 439 Agricultural and forest meteorology 178:10-20
- 440 Schneider U, Becker A, Finger P, Meyer-Christoffer A, Rudolf B, Ziese M (2015) GPCP full data reanalysis version
- 441 7.0 at 0.5: monthly land-surface precipitation from rain-gauges built on GTS-based and historic data.
- 442 FD\_M\_V6\_050 doi:10.5676/DWD\_GPCC\_FD\_M\_V7\_050
- 443 Schrier G, Barichivich J, Briffa KR, Jones PD (2013) A scPDSI - based global data set of dry and wet spells for
- 444 1901&ndash;2009. Journal of Geophysical Research Atmospheres 118:4025-4048
- 445 Shen J (2008) Meteorological disasters dictionary of China: vol. Inner Mongolia. . Eteorological Press, Beijing (in
- 446 Chinese)
- 447 Shindell D, Rind D, Balachandran N, Lean J, Lonergan P (1999) Solar cycle variability, ozone, and climate. Science
- 448 284:305-308
- 449 Shuai J, Zhang Z, Tao F, Shi P (2016) How ENSO affects maize yields in China: understanding the impact
- 450 mechanisms using a process - based crop model. International Journal of Climatology 36:424-438
- 451 Sun J, Wang H, Yuan W (2008) Decadal variations of the relationship between the summer North Atlantic Oscillation
- 452 and middle East Asian air temperature. Journal of Geophysical Research: Atmospheres 113
- 453 Sun J, Liu Y (2013) Drought variations in the middle Qilian Mountains, northeast Tibetan Plateau, over the last 450
- 454 years as reconstructed from tree rings. Dendrochronologia 31:279-285
- 455 Sun Y (2007) Meteorological disasters dictionary of China: vol. Heilongjiang. Eteorological Press, Beijing, China
- 456 Trouet V, Esper J, Graham NE, Baker A, Scourse JD, Frank DC (2009) Persistent positive North Atlantic Oscillation
- 457 mode dominated the medieval climate anomaly. science 324:78-80
- 458 Wang B, Liu J, Kim H-J, Webster PJ, Yim S-Y, Xiang B (2013) Northern Hemisphere summer monsoon intensified
- 459 by mega-El Niño/southern oscillation and Atlantic multidecadal oscillation. Proceedings of the National
- 460 Academy of Sciences 110:5347-5352
- 461 Wang X, Brown PM, Zhang Y, Song L (2011) Imprint of the Atlantic multidecadal oscillation on tree-ring widths in
- 462 Northeastern Asia since 1568. Plos One 6:e22740
- 463 Wang X, Song L (2011) Climate-tree growth relationships of *Pinus sylvestris* var. *mongolica* in the northern
- 464 Daxing'an Mountains, China. Chinese Journal of Plant Ecology 35:294-302
- 465 Wang X, Lv S (2012) Tree-ring reconstructions of January-March streamflow in the upper Nenjiang River since
- 466 1804, China. Arid Land Geography 4:002
- 467 Wang X, Li Z, Ma K (2014) Decreased sensitivity of tree growth to temperature in Southeast China after the 1976/'77
- 468 regime shift in Pacific climate. Sains Malaysiana 43:9-19
- 469 Wang Y et al. (2005) The Holocene Asian monsoon: links to solar changes and North Atlantic climate. Science
- 470 308:854-857
- 471 Wigley TM, Briffa KR, Jones PD (1984) On the average value of correlated time series, with applications in
- 472 dendroclimatology and hydrometeorology. Journal of climate and Applied Meteorology 23:201-213
- 473 Xu H (1998) Daxing'an Mountains Forests in China Science Press, Beijing, China
- 474 Yao Q et al. (2017) Pacific - Atlantic Ocean influence on wildfires in northeast China (1774 to 2010). Geophysical
- 475 Research Letters
- 476 Zhao H, Zhao X, Zhang T, Zhou R (2002) Boundary line on agro-pasture zigzag zone in north China and its problems
- 477 on eco-environment. Advances in Earth Science 17:739-747
- 478 Zhu L, Li Z, Zhang Y, Wang X (2017) A 211-year growing season temperature reconstruction using tree-ring width in
- 479 Zhangguangcai Mountains, Northeast China: linkages to the Pacific and Atlantic Oceans. International
- 480 Journal of Climatology 37:3145-3153 doi:10.1002/joc.4906



481 **Tables**

482 **Table 1** Information of the weather stations and gridded data nearest to sampling sites.

Site	Lat (N)	Lon (E)	Alt (m)	Time-Span, AD	Size
Xiaoergou	49°12'	123°43'	286.1	1957-2014	—
TS3.23 Mean T	51.25°	123.75°	-	1901-2014	0.5°*0.5°
GPCC Precipitation	51.25°	123.75°	-	1901-2014	2.5°*2.5°
Dai-PDSI	51.25°	123.75°	-	1911-2013	2.5°*2.5°
Cook-PDSI	51.25°	123.75°	-	1725-2005	2.5°*2.5°
sc-PDSI	51.25°	123.75°	-	1901-2013	0.5°*0.5°
CSIC-SPEI	51.25°	123.75°	-	1901-2012	0.5°*0.5°

483



484 **Table 2** Site description and statistical characteristic for the *Pinus sylvestris* chronologies in the Daxing'an Mountains.

Site	Lat. (N)	Long. (E)	Elev. (m)	No. of trees	Time span	EPS <sup>a</sup>	Rbar <sup>b</sup>
Keyihe (KY)	50°39'44.8"	122°23'13.3"	550	36	1725-2010	0.93	0.57
Alihe (AL)	50°38'37.7"	124°28'28.7"	380	32	1742-2010	0.87	0.52
Ganhe (GH)	50°43'51.9"	123°05'56.9"	760	19	1793-2010	0.88	0.59
Jinhe (JH)	50°26'16.7"	121°59'46.7"	830	33	1769-2011	0.95	0.61
Region (RE)	-	-	-	-	1725-2010	0.97	0.51

485 <sup>a</sup> Expressed population signal statistic.

486 <sup>b</sup> Rbar = the mean correlation coefficient between all tree-ring series used in a chronology.



487 **Table 3** Five-chronology correlation matrix over the common period 1793–2010.

	AL	GH	JH	Region
KY	0.38**	0.46**	0.55**	0.81**
AL		0.33**	0.32**	0.68**
GH			0.32**	0.72**
JH				0.74**

488 \*\* Significance level ( $p < 0.01$ ). The site codes are identical with those in Table 2.



489 **Table 4** Calibration and verification statistics for the PDSI reconstruction

Calibration	$r$	Verification	$R^2$	RE	CE	ST	PMT	RMSE
1911-2010	0.62**	-	-	0.38	-	(74, 26)**	8.04**	1.4
1961-2010	0.53**	1911-1960	0.47**	0.47	0.47	(39, 11)**	5.24**	1.34
1911-1960	0.69**	1961-2010	0.28**	0.28	0.25	(34, 16)*	6.23**	1.25

490 \* =  $p < 0.05$ , \*\* =  $p < 0.01$ .



491 **Table 5** Reconstructed extreme dry/wet years and annual PDSI of the Daxing'an Mountains.

Dry_year (Rank)	PDSI	Dry_year (Rank)	PDSI	Wet_year (Rank)	PDSI
1784 (1)	-3.574	1909 (16)	-2.484	1998 (1)	2.521
1853 (2)	-3.315	1916 (17)	-2.479	1952 (2)	2.091
1818 (3)	-3.238	1854 (18)	-2.405	1770 (3)	2.020
1862 (4)	-3.006	1865 (19)	-2.314	1993 (4)	2.011
1863 (5)	-3.001	1861 (20)	-2.310	1766 (5)	1.790
1918 (6)	-2.991	1864 (21)	-2.283	1897 (6)	1.728
1919 (7)	-2.977	1856 (22)	-2.275	1996 (7)	1.663
1915 (8)	-2.882			1899 (8)	1.655
1917 (9)	-2.777			1755 (9)	1.576
1852 (10)	-2.733			1999 (10)	1.548
1851 (11)	-2.716			2000 (11)	1.488
1860 (12)	-2.695			1997 (12)	1.451
1967 (13)	-2.671			1994 (13)	1.422
1925 (14)	-2.660			1769 (14)	1.405
1911 (15)	-2.581			1764 (15)	1.279

492

493



494 **Table 6** The long-term droughts and pluvial in the Daxing'an Mountain during the last 260 years.

Year	Dry/Wet	Duration	Magnitude	Intensity
1751-1752	Dry	2	-2.36	-1.33
1757-1771	Wet	15	19.52	1.30
1812-1817	Dry	6	-3.73	-0.62
1847-1866	Dry	20	-32.70	-1.64
1881-1902	Wet	22	18.98	0.86
1906-1927	Dry	20	-31.79	-1.59
1952-1955	Wet	4	2.78	0.69
1989-2004	Wet	16	19.67	1.23

495



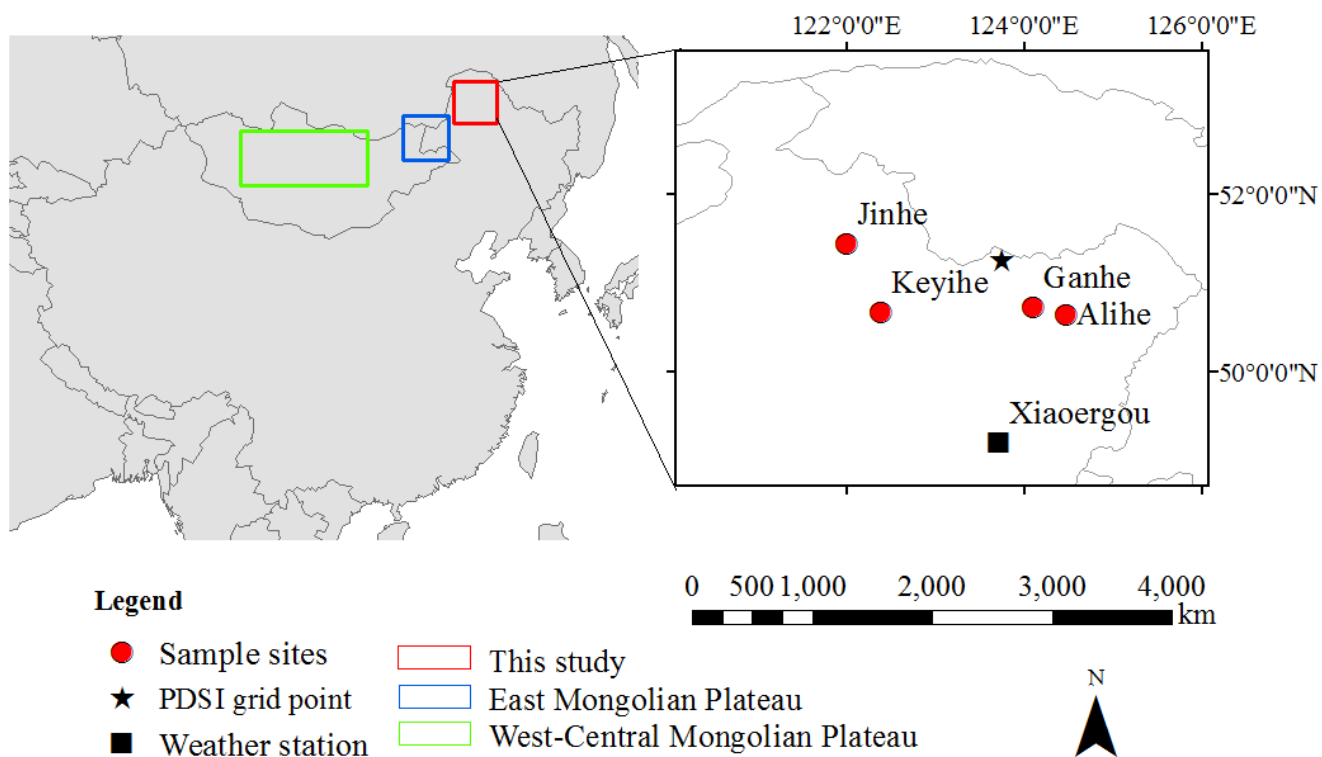
496 **Table 7** Correlation coefficients between large-scale climate and local annual mean temperature, total precipitation, actual Dai-PDSI  
 497 as well as the Z-score of dry/wet variation among the Daxing'an Mountains ( $DM_{Z-score}$ )

	Temperature			Precipitation			PDSI			$DM_{Z-score}$		
	<i>R</i>	<i>p</i>	N	<i>R</i>	<i>p</i>	N	<i>R</i>	<i>p</i>	N	<i>R</i>	<i>p</i>	N
AMO	0.44**	0.00	106	0.30**	0.00	106	0.44**	0.00	96	0.35**	0.00	282
PDO	0.46**	0.00	106	0.39**	0.00	106	0.51**	0.00	96	0.34**	0.00	282
NAO	0.17	0.08	106	-0.04	0.71	106	-0.08	0.43	96	-0.21**	0.00	282
SNAO	0.22*	0.02	110	0.08	0.39	110	0.08	0.42	100	0.13*	0.05	246
TSI	0.23*	0.01	110	0.35**	0.00	110	0.34**	0.00	100	0.12*	0.04	286
Niño 3	0.34**	0.00	106	0.26**	0.01	106	0.28**	0.01	96	0.14**	0.02	282

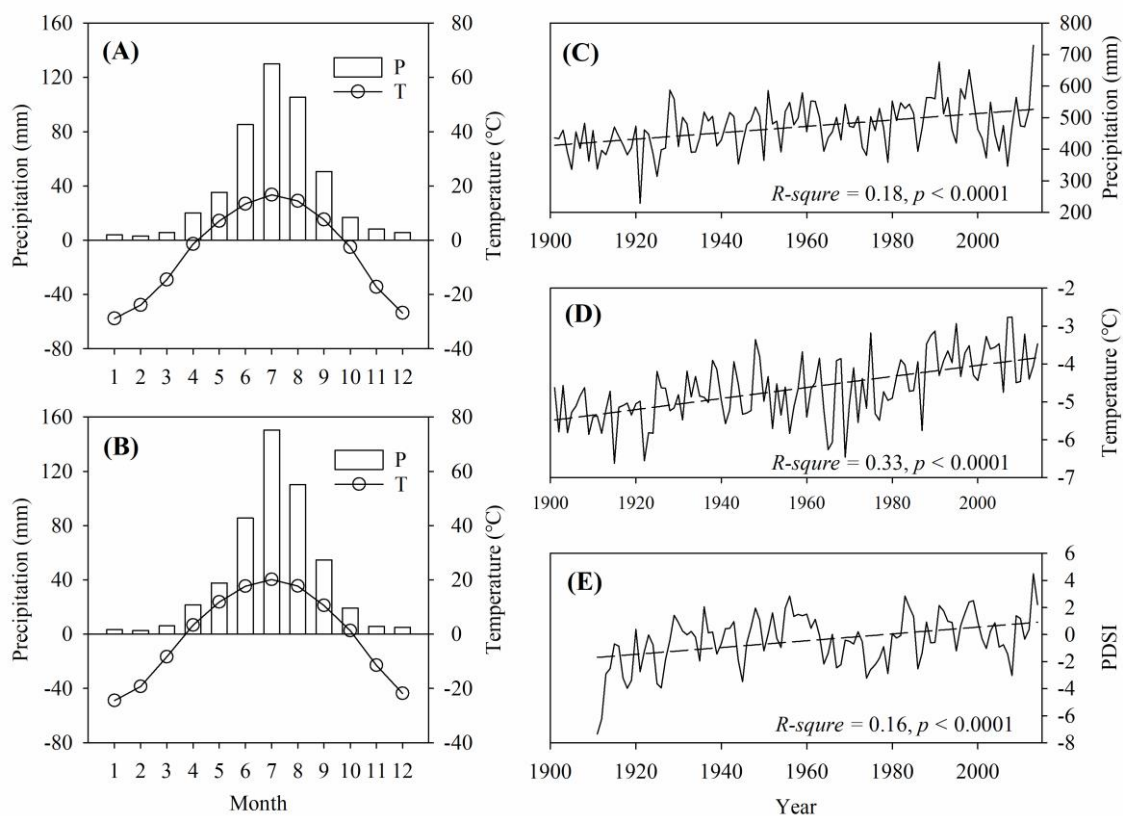
498 Note: The AMO, PDO, NAO, SNAO, TSI and Niño 3 are refer to the Atlantic Multidecadal Oscillation reconstruction from Mann  
 499 et al. (2009), the Pacific Decadal Oscillation reconstruction from Mann et al. (2009), , the Multi-decadal Winter North Atlantic  
 500 Oscillation reconstruction from Trouet et al. (2009), the summer NAO based on the 20C reanalysis sea-level pressure reconstruction  
 501 (SNAO), the Total Solar Irradiance reconstruction from IPCC AR5 and the Niño 3 reconstruction from Mann et al. (2009). All above  
 502 data were downloaded from <http://climexp.knmi.nl/>. \*  $p < 0.05$ , \*\*  $p < 0.01$



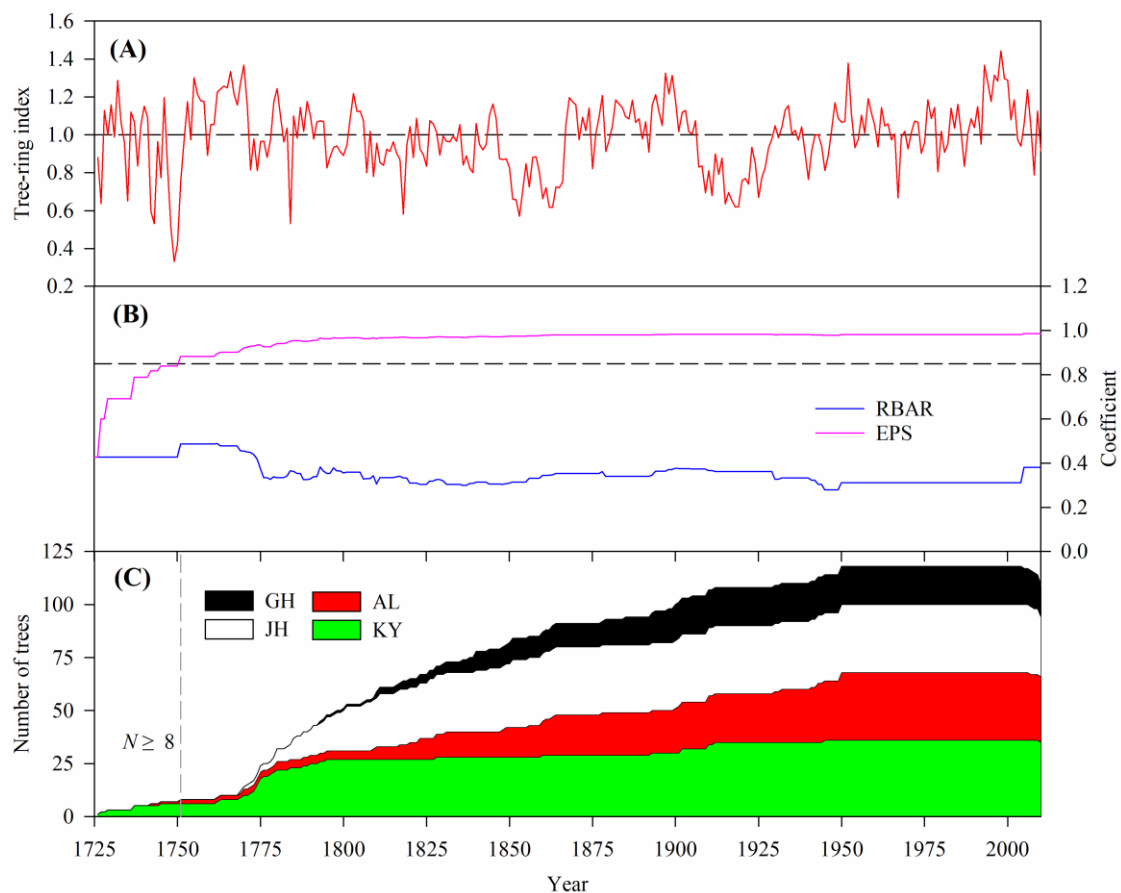
503 **Figures**



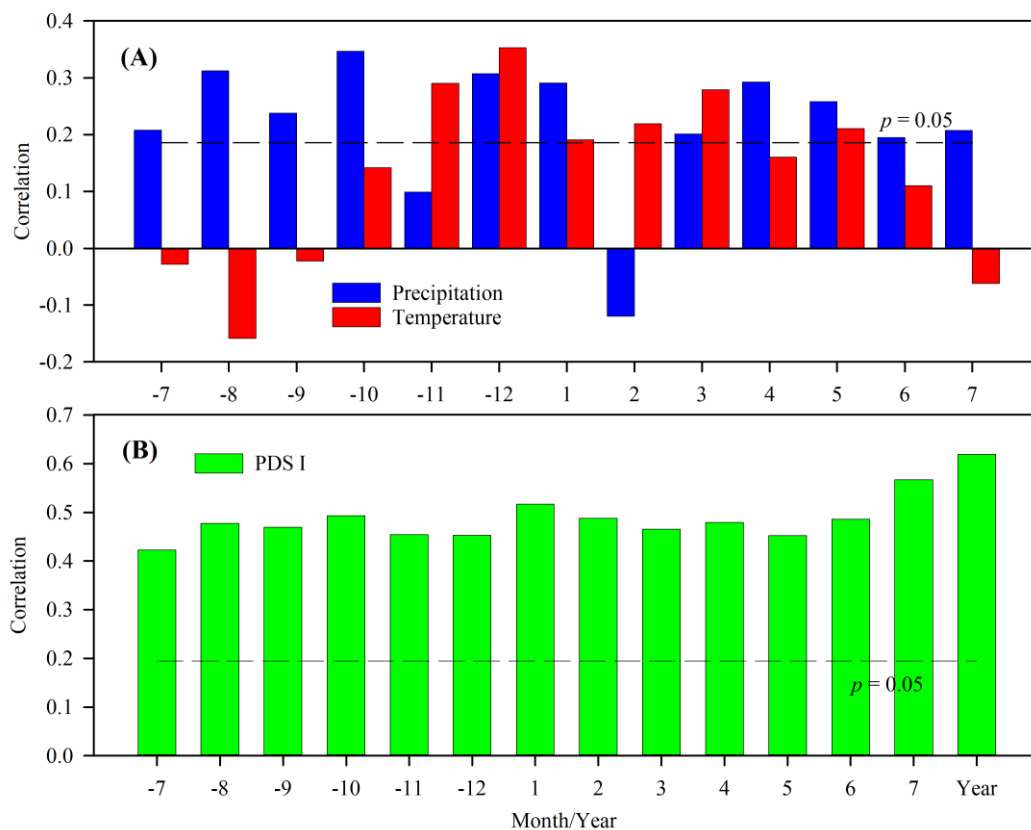
504  
505 **Fig. 1: Sampling sites and weather station distribution map.**



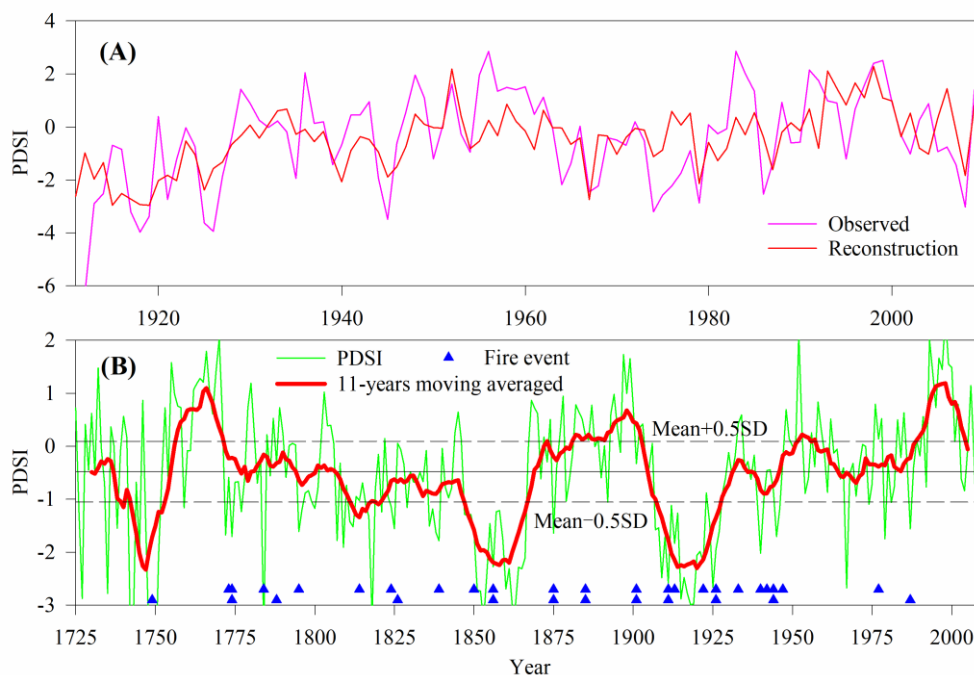
506  
 507 **Fig. 2: Monthly sum of precipitation (P) and mean temperature (T) of the Xiaogou (A) meteorological station (1957–2014)**  
 508 **and grids (B) data (1901-2014); the sum of annual precipitation (C), and the average of annual temperature (D) and**  
 509 **PDSI (E). The dashed line indicates the linear fitting values.**



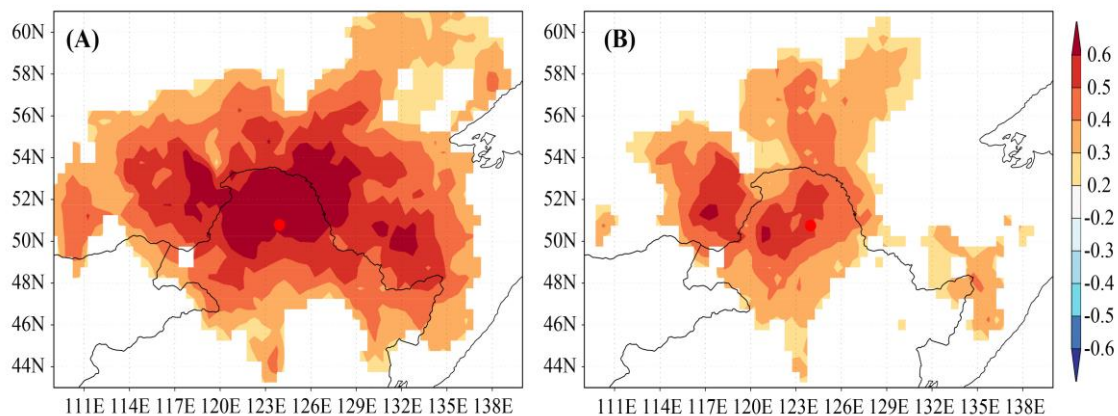
510  
511 **Fig. 3:** The regional tree-ring width chronology of *Pinus sylvestris* in the Daxing'an Mountains . (B) The RBAR, EPS, and  
512 (C) sample size for the chronology are also shown. RBAR and EPS are computed using 51-year windows. The reliable  
513 portion of the chronology is determined by the EPS value > 0.85.



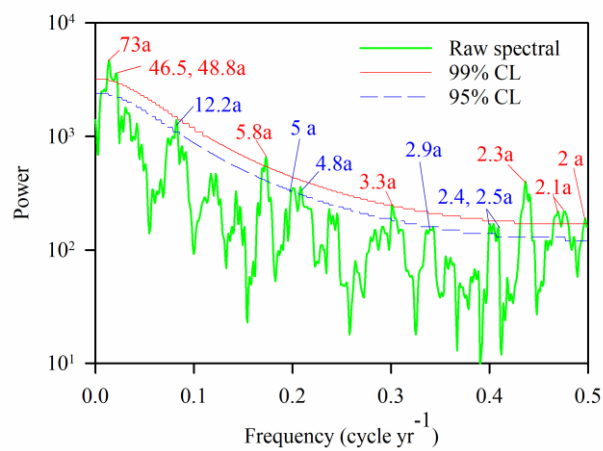
514  
 515 **Fig. 4: Pearson correlation coefficients between tree-ring index of *Pinus sylvestris* and monthly total precipitation, mean**  
 516 **temperature (A) and Dai-PDSI (B). Significant correlations ( $p < 0.05$ ) are indicated by dash lines. The letter “-” in**  
 517 **abscissa represents the previous year.**



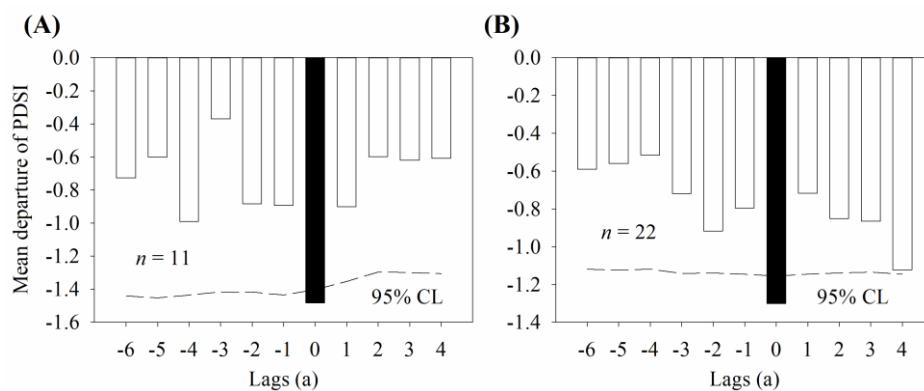
518  
519 **Fig. 5: PDSI reconstruction in the Daxing'an Mountains, northeast China. (A) Comparison of the observed and**  
520 **reconstructed annual PDSI during the calibration period 1911-2010; (B) Tree-ring reconstruction of annual PDSI,**  
521 **plotted annually from 1725 to 2010 (cyan line), along with a smoothed 11-year moving average (red line); Blue filled**  
522 **triangles indicate nearby regionally forest fire event records reconstructed by tree-ring scars from Mengkeshan (down)**  
523 **and Pangu (up).**



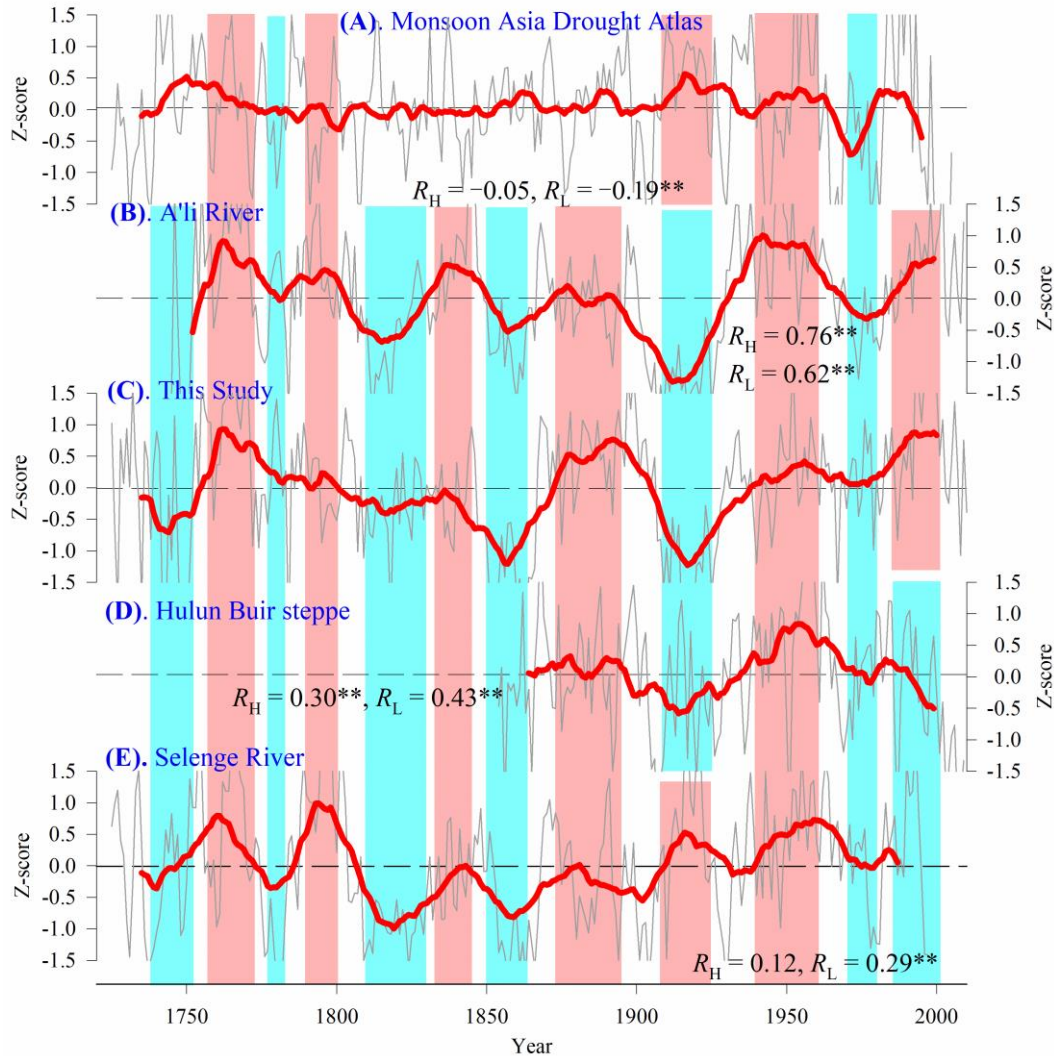
524  
525 **Fig. 6: Spatial correlation fields of (A) actual and (B) reconstructed annual Dai-PDSI for the Daxing'an Mountain with**  
526 **regional grided scPDSI for the period 1911–2010 (<http://climexp.knmi.nl/>).**



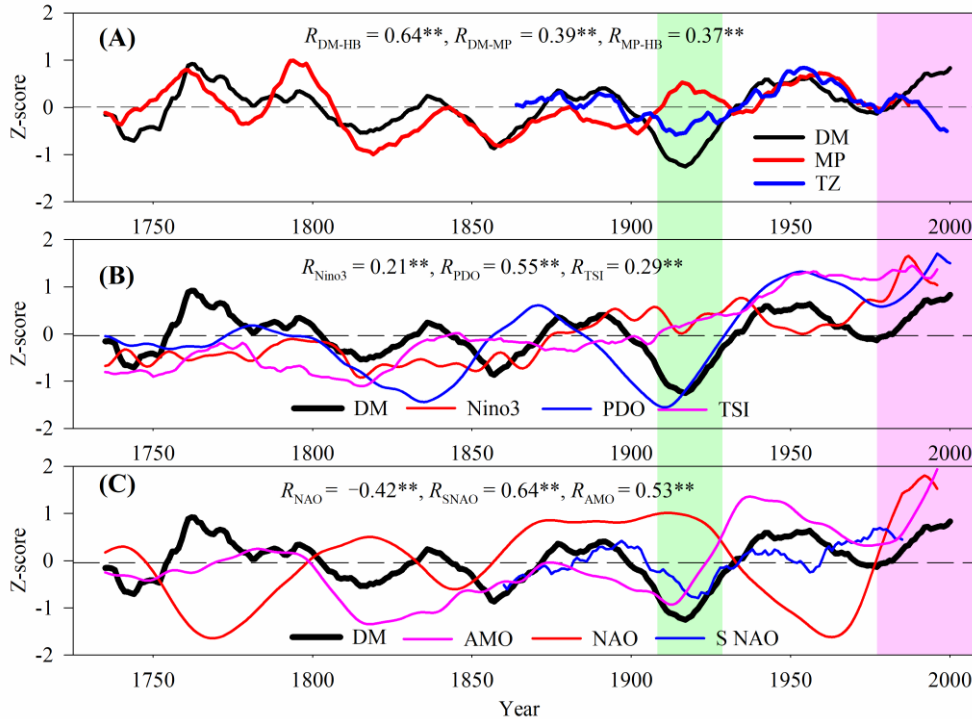
527  
528 **Fig. 7: Multi-taper method power spectrum of reconstructed Dai-PDSI for the period AD 1751-2010. The 95% and 99%**  
529 **confidence level relative to red noise are shown and the numbers refer to the significant period in years.**



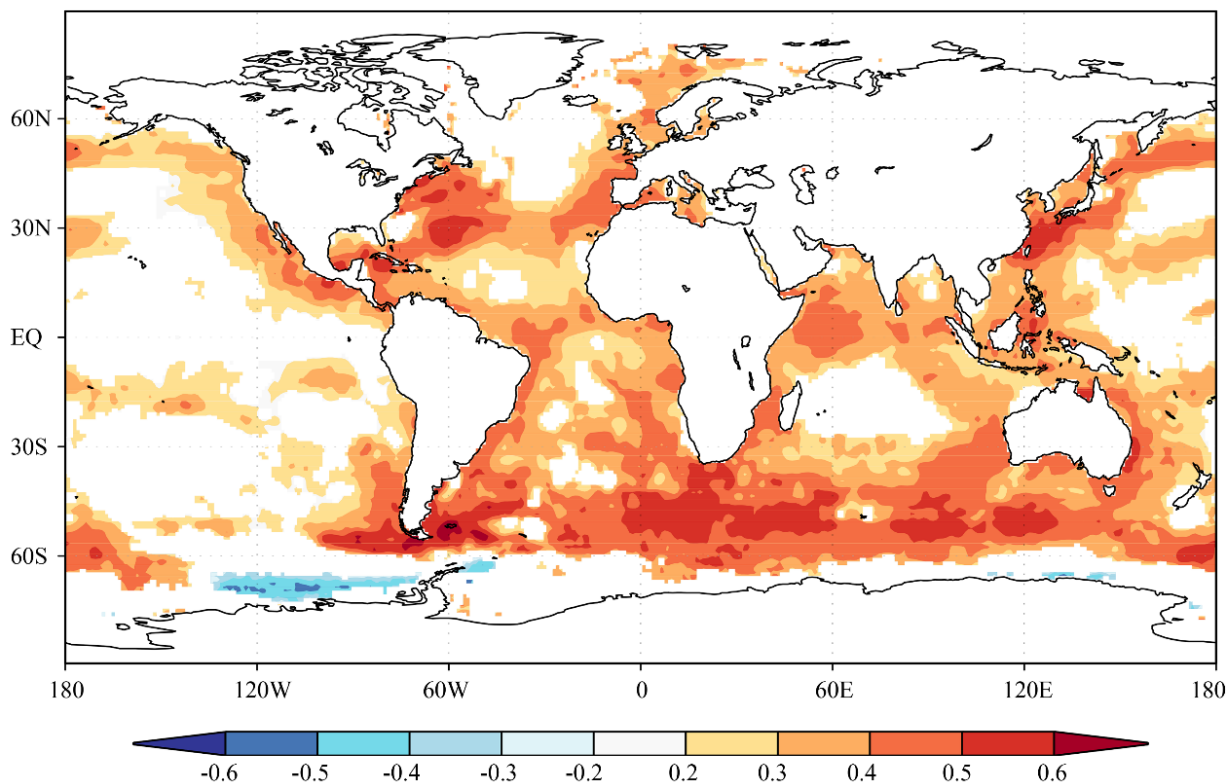
530  
531 **Fig. 8:** Superposed epoch analyses of reconstructed Dai-PDSI (1751-2010) with regional wildfire years of (A) Mengkeshan  
532 (1743-2010) and (B) Pangu (1767-2010) in the Daxing'an Mountains, northeast China. The analysis window includes six  
533 years before and four years after each fire year (year "0"). Black bars mark statistically significant departures ( $p < 0.05$ ;  
534 dashed lines) from mean conditions.



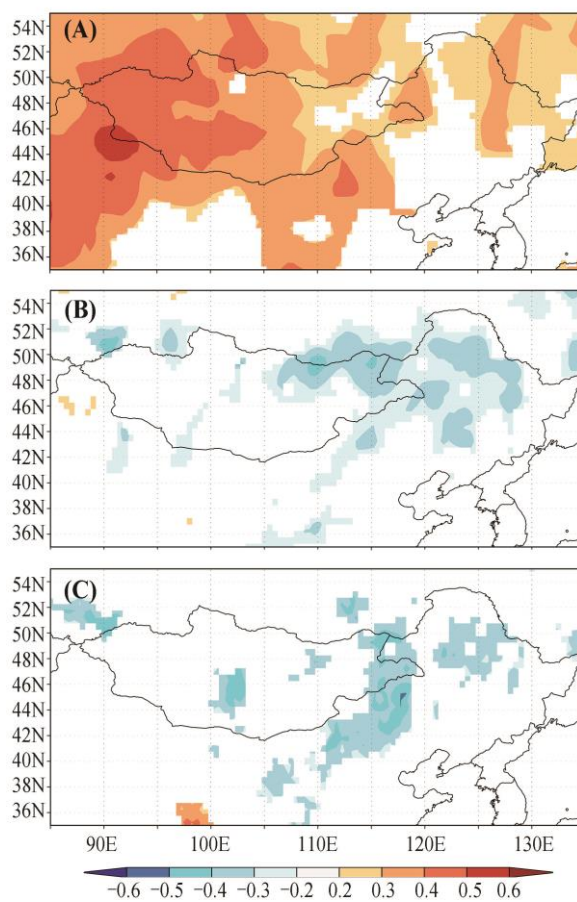
535  
 536 **Fig. 9: Comparisons of (A) drought reconstruction of “Cook” from same PDSI grid derived from the Monsoon Asia Drought**  
 537 **Atlas (MADA, Cook et al. (2010)), (B) Winter precipitation reconstruction of the A’li River in northeastern China (AR,**  
 538 **Lv and Wang (2014)), (C) the mean annual PDSI reconstruction for the Daxing’an Mountain (TS, in this study), (D)**  
 539 **April–August SPEI reconstruction of the Hulun Buir steppe in eastern Mongolian Plateaus (HB, Bao et al. (2015)) and**  
 540 **(E) April–October streamflow reconstruction of the Selenge River in northeastern Mongolia (SR, Davi et al. (2006)). All**  
 541 **above series were standardized using Z-scores (high frequency) and then smoothed with a 21-year moving averaged**  
 542 **(low frequency; red bold line). Blue (dry) and red (wet) shading are low and high PDSI zones with good agreements.**  
 543 **Correlation coefficients in low ( $R_L$ ) and high ( $R_H$ ) frequency are listed in the figure.  $** p < 0.01$**



544  
 545 **Fig. 10: Comparisons of drought reconstruction and other large-scale climate system cycles. (A), dry/wet variation among**  
 546 **the Daxing'an Mountains (average of our reconstruction and the precipitation reconstruction of the A'li River), the**  
 547 **Mongolian Plateaus (streamflow reconstruction of the Selenge River) as well as their transition zones (SPEI**  
 548 **reconstruction of the Hulun Buir steppe); (B), the drought reconstruction of the Daxing'an Mountains, the Pacific**  
 549 **Decadal Oscillation and the Niño 3 index reconstruction from Mann et al. (2009) as well as the Total Solar Irradiance**  
 550 **reconstruction from IPCC AR5; (C) the drought reconstruction of the Daxing'an Mountains, the Atlantic Multidecadal**  
 551 **Oscillation reconstruction from Mann et al. (2009), the Multi-decadal Winter North Atlantic Oscillation reconstruction**  
 552 **from (Trouet et al. (2009)) and the summer NAO based on the 20C reanalysis sea-level pressure reconstruction (SNAO).**  
 553 **All above series were standardized using Z-scores and then smoothed with a 21-year moving averaged to highlight low-**  
 554 **frequency drought signals. Significant correlation coefficients (\*\*  $p < 0.01$ ) are listed in the figure.**



555  
556 **Fig. 11: Spatial correlations between estimated temperature with sea surface temperature in global scale. The spatial**  
557 **correlation was carried out for annual PDSI covering a time span from AD 1911 to 2010.**



558  
559 **Fig. 12: Spatial correlations between annual East Asian monsoon indexes with local (A) temperature, (B) precipitation and**  
560 **(C) scPDSI from AD 1948 to 2010.**